

Radiative sky cooling in low-medium concentration photovoltaic systems

Yingfeng Li^{*}, Laiyu Zhang, Wenxiang Gao, Yingjian Liu, Jiayuan An, Zhihan Liu, Xing Ju, Meicheng Li^{*}

^a State Key Laboratory of Alternate Electrical Power System with Renewable Energy Sources, North China Electric Power University, Beijing 102206, China

ARTICLE INFO

Keywords:

Radiative sky cooling
Low-medium concentration photovoltaics
Passive heat dissipation

ABSTRACT

Low-medium concentration photovoltaics (LM-CPV) can significantly reduce cost by using cheap optical lenses to reduce the area of the solar cell. Recently, radiative sky cooling (RSC) has been demonstrated to be promising for CPV systems. However, in the reported designs of heat dissipation for CPV systems combining the radiative cooler and a heat sink, a simple flat heat sink was used. Therefore, the effect of the radiative heat dissipation was magnified, but the contribution of convection, which accounts for a significant share in the natural working environment of CPV, was inhibited. To give full play to the role of convection, in this paper, a heat dissipation design combining a radiative cooling layer (RCL) and a finned heat sink was proposed. The RCL was laid on the upper surface of the heat sink to enhance heat dissipation for RSC and realize the effects of thermal radiation. The contributions of the RCL in reducing the temperature of the device, heat dissipation, and obtaining a tolerable concentration ratio under different external environments were examined, and the law whereby the cooling effect of the RCL was influenced by the wind speed and ambient temperature was investigated. The results of numerical simulations shown that the proposed passive cooling device could ensure that the temperature of the solar cell did not exceed 71.5 °C at a concentration ratio of 200, and the maximum difference in temperature inside the device was less than 3.8 °C even in extremely harsh environments (wind speed, 0 m/s; ambient temperature, 50 °C), where this satisfies the requirements of heat dissipation in low-medium concentration silicon solar cells. The radiative heat dissipation power per unit area of the RCL was 201 W/m², far exceeding the convective heat dissipation. Although the area of the RCL only accounted for 7.9 % of the total area of heat dissipation, its radiative ratio of heat dissipation exceeded 15 % of the total heat dissipation and led to a drop in temperature of 1.76 °C. Moreover, the increase in ambient wind speed significantly improved the cooling effect of the device, which could ensure the rise in the temperature of the solar cell relative to the environment to smaller than 5 °C. However, this also diluted the effect of radiative heat dissipation by the RCL. The increase in the ambient temperature significantly improved the ratio of radiative heat dissipation of the RCL to the overall heat dissipation, reaching 20.2 % when the concentration ratio was 100. In all cases, the cooling power per unit area of the RCL was higher than that of convective and conventional radiative heat dissipation. An even better cooling effect could be achieved by further increasing the relative area of the RCL. Finally, we found that the maximum acceptable concentration ratio of the device was approximately linearly related to the size of the heat sink, and using the RCL could enable the device to withstand an additional 10 ~ 15 multiples of concentration. The work here provides a new technical option for reducing the cost and improving the efficiency of photovoltaic power generation through the systematic exploration of the influence of the RSC on cooling LM-CPV systems.

1. Introduction

Concentrated photovoltaic (CPV) technology uses cheap optical units to replace most of the area of the solar cell, and is expected to provide new space for photovoltaic power generation to increase its efficiency and reduce cost. As early as in 2012, Intelligent Manufacturing Systems

(IMS) Research predicted that low-medium concentration photovoltaics (LM-CPV) based on crystalline silicon solar cells have significant potential for development [1]. Compared with flat silicon solar cells, concentrated silicon solar cells have significant advantages in terms of efficiency, cost, and environmental adaptability. Their maximum efficiency (27.6 %±1.2 % [2]) is still well below the theoretical limit of 37

^{*} Corresponding authors.

E-mail addresses: liyinfeng@ncepu.edu.cn (Y. Li), mcli@ncepu.edu.cn (M. Li).

<https://doi.org/10.1016/j.applthermaleng.2022.119860>

Received 18 July 2022; Received in revised form 24 October 2022; Accepted 9 December 2022

Available online 17 December 2022

1359-4311/© 2022 Elsevier Ltd. All rights reserved.

% [3]. The higher the concentration ratio, the lower the cost of the device, the better its performance in poor light, and the smoother the curve of its output power. In an area with low solar irradiance and an average annual light intensity of 200 W/m^2 , the efficiency of flat silicon solar cells is reduced by 15 %–30 % [4], but this problem can be solved by using concentrated technology. Given that there is no more room for improving the efficiency and reducing the cost of flat-panel silicon solar cells, concentrated silicon photovoltaics are expected to be the focus of research on photovoltaic power generation again [5].

Heat dissipation is a major challenge to the development of concentrated silicon solar cells. When the concentration ratio was 200, the heat-generating power P_{heat} by the silicon solar cell can be evaluated by: $P_{\text{heat}} = 200 \times P_{\text{in}} \times (1 - \eta_{\text{pv}})$. If we assume the solar irradiance P_{in} equals to 1000 W/m^2 and the photoelectric conversion efficiency of the silicon solar cell is 27 %, the heat-generating power should be about $1.46 \times 10^5 \text{ W/m}^2$. Not only did the temperature rise degrade the efficiency of the cell at a rate of $0.4 \text{ \%}/^\circ\text{C}$ [6], but silicon solar cells could also be oxidized or even burned up within minutes in this case [7]. Therefore, developing of low-cost, highly reliable, powerless, and maintenance-free heat dissipation technology is important for low-medium concentration silicon solar cells.

Radiative sky cooling (RSC) is a passive cooling technology that has received considerable attention in recent years [8–16]. It involves releasing terrestrial heat in the form of radiation through an “atmospheric window” of 8–13 μm electromagnetic waves into cosmic space at temperatures close to absolute zero. To realize RSC in general, special materials and structures, such as refractive index matching and ultra-broadband micro-nano-structures or photonic crystals, are used to achieve low surface emissivity in the 0.3–8 μm band and high surface emissivity (close to one) in the 8–13 μm band [17–23]. RSC is a promising method to passively cool photovoltaic cells under outdoor conditions [24–26]. Fan et al. used sky radiation materials to dissipate heat in flat silicon solar cells, and predicted that this technology could reduce the temperature of solar cells by $18.3 \text{ }^\circ\text{C}$ [27]. Fan et al. subsequently developed various materials for sky radiation that can reduce the temperature of flat silicon solar cells by $13 \text{ }^\circ\text{C}$ [28–29]. Wang and Pei et al. have reduced the temperature of the commercial silicon cells by $2 \text{ }^\circ\text{C}$ and $3.6 \text{ }^\circ\text{C}$, using a pyramid-textured PDMS film and a micro-grating photonic cooler, respectively [30–31].

RSC is also promising to be explored for concentrated photovoltaics (CPV) systems [32]. However, as the net cooling power per unit area of RSC at room temperature is only about 150 W/m^2 , [12,33] which cannot satisfy the requirements of heat dissipation of CPV systems, it is usually necessary to lay the radiative cooler on the heat sink with a larger area than the solar cell. For example, Sun et al. have designed a reflective CPV system with a large flat heat and demonstrated that a radiative cooler on the top facing towards the sky could reduce the temperature of the solar cell by $14 \text{ }^\circ\text{C}$ [34]. Besides, since the cell temperature in a CPV system is usually higher than the ambient temperature, adding a radiative cooler on the heat sink’s rear surface can also enhance thermal radiation exchange with the ground. Therefore, Wang et al. have pasted radiative coolers on both the top and bottom of the heat sink in a GaSb CPV system, achieving a $36 \text{ }^\circ\text{C}$ temperature drop and a 31 % relative increase of open-circuit voltage [35].

The above heat dissipation designs for CPV systems mainly emphasized the effect of the radiative cooler, so a simple flat heat sink with weak convection cooling was used. However, in most cases, there is a certain wind speed in the outdoor environment; [35,32] and even using flat heat sinks, the radiative heat dissipation was significantly diluted with increasing wind speed [36,37,24]. This means that in the actual work environment, the convective heat dissipation will account for a large share; and it should be more practical to combine the radiative cooler and finned heat sink with more vigorous convection heat dissipation effect in a CPV system. Besides, it has been demonstrated that quick and efficient heat transfer throughout 0.5 m can be achieved using a heat pipe [38]. Therefore, we propose a passive heat dissipation device

for low-medium concentration silicon solar cells based on the design of the point-focusing CPV system, where the silicon solar cells are connected to flat heat pipes (vapor chambers, VC) through thermal interface material (TIM), the flat heat pipes are welded to the heat sink, and the radiative cooling layer (RCL) is laid on the upper surface of the heat pipe and the heat sink excluding the solar cell. In our CPV system, the incident light is concentrated on the solar cells by a condenser lens, and the area under the lens, excluding the solar cell, is not directly irradiated by sunlight; therefore, there is no transparency requirement for the RCL, only its high emissivity in the atmospheric window band is required [32,35].

In the existing research, either the concentration multiple is fixed [35], or only the effect of the concentration multiple on the overall temperature reduction is investigated without considering the impact of concentration multiple on various forms of heat dissipation [34]. Furthermore, there are few reports exploring the effect of ambient temperature on heat dissipation. This study used a steady-state heat transfer simulation to examine whether the above design of the device could satisfy the requirements of heat dissipation of concentrated silicon solar cells under a variety of external conditions. The authors focused on the effects of RSC on the reduction in temperature, heat dissipation, and the contribution to the maximum acceptable concentration ratio for LM-CPV. The influence of concentration multiple, wind speed and ambient temperature on the sky radiation effect was also investigated. The results shown that our cooling device based on RSC and the heat sink could satisfy the requirements of heat dissipation of low-medium concentration silicon solar cells even in extremely harsh environments.

2. Methodology

The research here was based on the finite element analysis (FEA) module of the commercial software COMSOL-Multiphysics 5.6. Model building and finite element calculations were performed directly in the COMSOL software.

2.1. Proposed model

A schematic diagram of a point-focusing CPV system is shown in Fig. 1. Incoming sunlight is concentrated by a concentrator and then irradiated on the silicon solar cell. The solar cell is connected to the vapor chambers (VC) through TIM, and the VC is welded to the heat sink. The radiative cooling layer (RCL) is laid on the upper surface of the VC and the heat sink, excluding the solar cell. Harmful heat in the solar cell is conducted to the VC through the TIM and further to the heat sink. The device releases heat to the environment in the form of convection and thermal radiation.

The model of the cooling device includes solar cells, TIM, VC, heat sinks, and a radiative cooling layer (RCL). We assumed that the solar cell was a single monocrystalline silicon cell that was not covered by any other material, such as glass or metal grid lines. The TIM was assumed to have a thickness of about $100 \mu\text{m}$, and its thermal conductivity was set to $10 \text{ W/m}\cdot\text{K}$ and the emission coefficient to 1.0. The VC was a metal copper block with a uniform thermal conductivity closely fitted with the heat sink. The heat sink consisted of a substrate and fins. The substrate size was $107 \times 80 \text{ mm}^2$ with a thickness of 5 mm. There were 16 fins, each of which was 80 mm long, 33 mm high, and 2 mm thick. The distance between adjacent straight fins was 5 mm [39].

The RCL was a surface with no thickness, and its effect in terms of RSC was realized by wavelength-dependent surface emissivity. It was necessary to ensure high emissivity in the atmospheric window band (8–13 μm). The surface emissivities of the RCL were set to 0.05 at 0–2.5 μm , 0.1 at 2.5–4 μm , 0.9 at 4–8 μm , and 0.95 at 8–13 μm and beyond. The coefficients of thermal conductivity and thermal emissivity of the solar cell, VC, and heat sink were determined by the properties of the materials considered. The dimensional and physical parameters of each component in the device were given in Table 1. The value of ϵ of the Si

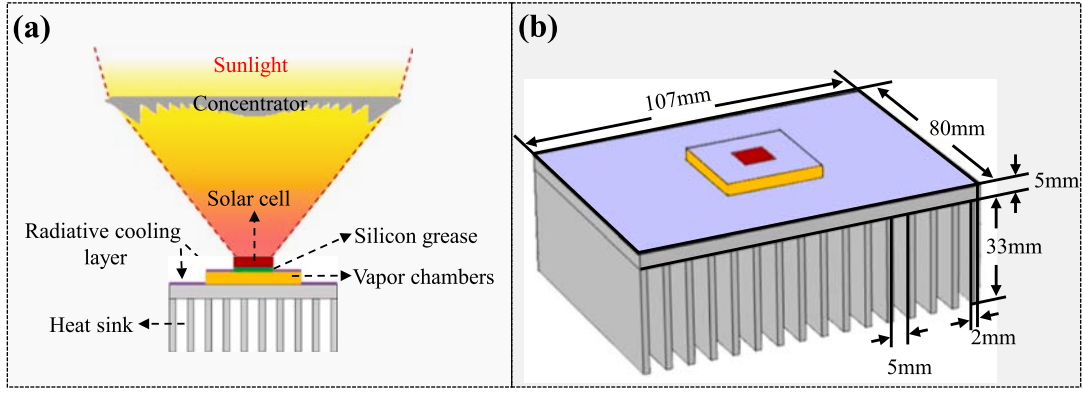


Fig. 1. Model of a point-focusing concentrated photovoltaic cooling device. (a) Point-focusing condensing and heat-dissipating device. (b) The dimensional parameters.

Table 1
Dimensions and physical parameters of each component of the cooling device.

Component	material	size (mm)	k (W/ m-K)	ε (a. u.)	C_p (J/ kg-K)	ρ (kg/ m ³)
Air	/	/	2.643 $\times 10^{-5}$	/	/	/
Solar cell	Silicon	10 \times 10 \times 0.2	131	0.65	700	2329
TIM	Silicon grease	10 \times 10 \times 0.1	10	1	1200	2600
Vapor chamber	Copper	30 \times 30 \times 4	700	0.6	385	8960
Heat sink	Aluminum	Fig. 1	238	0.4	900	2700
RCL	/	/	/	Fig. 2	/	/

solar cell comes from [36] those of the TIM, the vapor chamber, and the heat sink come from [40,41] the values of k of the TIM, the vapor chamber, and the air come from [42–44,52] respectively.

2.2. The environment

We used the heat-dissipating device as the object of our research. Under the assumption of point-focusing concentrated photovoltaics, the environmental factors of outdoor operation that we considered included the concentrated heat source, wind speed, and radiation from the environment directed toward the device.

We loaded the top surface of the solar cell in the numerical simulations with concentrated solar radiation in the form of boundary heat flux. We assumed that the solar irradiance Q_{rad} was 800 W/m², the concentration ratio (CR) varied from 1 to 200, and the loss of solar radiation η_{loss} caused by reflections of the concentrator and the solar cell was 7 %. The efficiency of photoelectric conversion η_{pv} of the silicon solar cell was 26 %, and solar radiation that entered the interior of the solar cells but was not converted into electricity was converted into “the harmful heat.” The flux of the heat source Q_{heat} on the surface of the solar cell was then calculated by [45]:

$$Q_{heat} = CR \times Q_{rad} \times (1 - \eta_{loss}) \times (1 - \eta_{pv}) \quad (1)$$

The wind speed u was used to determine the effect of convective heat transfer in the model. Natural convection with a wind speed of 0 m/s and forced convection with that >0 m/s were separately simulated. Eight cases of wind speed, $u = 0.0, 0.2, 0.5, 1.0, 1.5, 2.0, 2.5,$ and 3.0 (m/s), were investigated in total.

Ambient radiation to the model was determined by the ambient temperature T_{amb} and the ambient emissivity ε_{amb} . Cases with values of $T_{amb} = -10$ °C, -5 °C, 0 °C, 5 °C, 10 °C, 15 °C, 20 °C, 25 °C, 30 °C, 35 °C, 40 °C, 45 °C, and 50 °C were considered. Ambient emissivity ε_{amb} is also a function of wavelength λ . $\varepsilon_{amb} = 0.9$ in the $\lambda = 0$ – 2.5 μ m band, 0.8 in

the $\lambda = 2.5$ – 8 μ m band, and 0.2 in the $\lambda = 8$ – 13 μ m band. When $\lambda > 13$ μ m, $\varepsilon_{amb} = 0.9$ [12,24,27,46–51]. A comparison of the curves of ambient emissivity and the RCL is given in Fig. 2, where the cooling effect of RSC is described by the difference between $\varepsilon_{amb} = 0.2$ and $\varepsilon_{RCL} = 0.95$ in the 8–13 μ m band.

2.3. Theory and governing equations

The three basic modes of heat transfer within the device and between the device and the environment are conduction, convection, and radiation. Thermal conduction occurs inside the heat sink, and steady-state thermal conduction is described by the *Fourier* law, which defines the conductive heat flux q as being proportional to the temperature gradient ∇T :

$$q = -k\nabla T \quad (2)$$

where k is thermal conductivity [53].

Thermal convection occurs between the device and the environment. To reduce the calculation cost, both the natural and forced convection are solved by an empirical formula [54]:

$$q_0 = h(T - T_{amb}) \quad (3)$$

where q_0 is the convective heat flux, h is the coefficient of convective

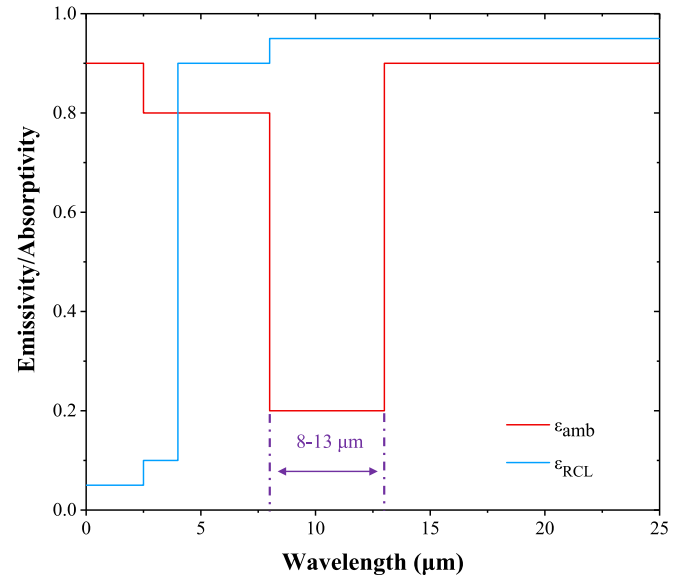


Fig. 2. Curves of ambient emissivity and the RCL emissivity.

heat transfer, T_{amb} is ambient temperature, and T is the model temperature.

We conducted simulations for two cases: natural and forced convection. The difference between them was reflected in the coefficient of convective heat transfer h , labeled h_{nat} and h_{for} , respectively. In natural convection, the surface of the model of the device was divided into three types according to its principle of heat dissipation: a vertical wall, and an upper surface and a lower surface of the horizontal plate. Boundary conditions were also set for them. The following formula was used to calculate the coefficient of heat transfer of natural convection by the vertical wall [54]:

$$h_{nat-ver} = \begin{cases} \frac{k}{L} \left(0.68 + \frac{0.67Ra_L^{1/4}}{\left(1 + (0.492k/\mu Cp)^{9/16}\right)^{4/9}} \right) & \text{if } Ra_L \leq 10^9 \\ \frac{k}{L} \left(0.825 + \frac{0.387Ra_L^{1/6}}{\left(1 + (0.492k/\mu Cp)^{9/16}\right)^{8/27}} \right)^2 & \text{if } Ra_L > 10^9 \end{cases} \quad (4)$$

where Ra_L is the Rayleigh number, L is the characteristic length, μ is hydrodynamic viscosity, Cp is the heat capacity at constant pressure, and k is thermal conductivity.

Ra_L is a dimensionless number used to characterize natural convection. It is expressed as the product of the Grashof number Gr and the Prandtl number Pr , where Gr represents the ratio of buoyancy to viscosity, and Pr represents the ratio of momentum diffusivity to thermal diffusivity [54]:

$$Ra_L = Gr \cdot Pr = \frac{\rho^2 g \alpha L^3 \Delta T}{\mu^2} \frac{C_p \mu}{k}, \quad (5)$$

where ρ is the density of the material, g is the acceleration due to gravity, and α is the coefficient of thermal expansion.

The coefficient of heat transfer due to natural convection on the upper and lower surfaces of the horizontal plate is as follows [54]:

$$h_{nat-up\&low} = \begin{cases} \frac{k}{L} 0.54Ra_L^{1/4} & \text{if } T > T_{ext} \text{ and } 10^4 \leq Ra_L \leq 10^7 \\ \frac{k}{L} 0.15Ra_L^{1/3} & \text{if } T > T_{ext} \text{ and } 10^7 \leq Ra_L \leq 10^{11} \\ \frac{k}{L} 0.27Ra_L^{1/4} & \text{if } T > T_{ext} \text{ and } 10^5 \leq Ra_L \leq 10^{10} \end{cases} \quad (6)$$

where T_{ext} is the external temperature.

In the case of forced convection with fluid velocity $u > 0$ m/s, no distinction is made between the types of thermal convection in different parts of the device. The coefficient of heat transfer due to forced convection is as follows [54]:

$$h_{for} = \begin{cases} 2 \frac{k}{L} \frac{0.338Pr^{1/3} Re_L^{1/2}}{\left(1 + (0.0468/Pr)^{2/3}\right)^{1/4}} & \text{if } Re_L \leq 5 \cdot 10^5 \\ 2 \frac{k}{L} Pr^{1/3} \left(0.037Re_L^{4/5} - 871\right) & \text{if } Re_L > 5 \cdot 10^5 \end{cases} \quad (7)$$

where Re_L is the Reynolds number [54].

$$Re_L = \frac{\rho u L}{\mu} \quad (8)$$

The physical parameters related to Eqs. (1)–(8) are given in Table 1, and L related to convective heat transfer is described in the next section.

Accounting for radiative heat dissipation requires considering the radiation between the surface of the device and the environment as well as radiation within the surface of the device itself. The former includes radiation from the environment to the device and that from the device to the environment. The radiation from the device to the environment is divided into radiation of the surface with the RCL and radiation of the surface without the RCL.

The contribution of any component of radiation can be described by the ideal gray-body radiation. The direction and magnitude of radiative heat flow are determined by the radiated area, the direction of radiation, and the coefficient of thermal emission. For an ideal grey body, the net inward radiative heat flux q_r is given by [55]:

$$q_r = G - J \quad (9)$$

where G is the incident irradiance and J is the radiative emission.

The incident irradiance G is given by the following [55] formula:

$$G = G_m + G_{amb} \quad (10)$$

G_m is radiation from other boundaries in the model, and was calculated by the program according to the geometry of the model. G_{amb} represents radiation from the environment and is defined as [54]:

$$G_{amb} = \varepsilon_{amb} F_{amb} e_b(T_{amb}) \quad (11)$$

where ε_{amb} is environmental emissivity, F_{amb} is the environmental perspective factor, calculated by the program according to the geometry of the model, and T_{amb} is the ambient temperature in the direction represented in F_{amb} .

For opaque surfaces, the emission J is given by the following formula [54]:

$$J = (1 - \varepsilon)G + \varepsilon e_b(T) \quad (12)$$

where ε is the surface emissivity of the cooling device (Table 1), $e_b(T)$ is the total power of transmission of the hemispherical black body that, according to the Stefan–Boltzmann law, depends on the temperature to the fourth power [54]:

$$e_b(T) = n^2 \sigma T^4 \quad (13)$$

where n is its refractive index, and σ is the Stefan–Boltzmann constant, $5.67 \cdot 10^{-8} \text{ W}/(\text{m}^2 \cdot \text{K}^4)$.

2.4. Boundary conditions and grid settings

We briefly introduce the main boundary conditions in Fig. 3. The boundary of heat flux Q_{heat} was set on the surface of the solar cell, and corresponded to different values under different concentration ratios. For devices with the RCL, we set wavelength-dependent emissivity functions ε_{amb} and ε_{RCL} on the surface of the RCL to achieve the RSC effect (Fig. 2).

In the case of natural convection, the surface of the device was divided into three types—the upper and lower surfaces of the horizontal plate, and the vertical wall—and their parameters were set accordingly. The characteristic length L was the main parameter considered. The characteristic lengths of the upper and lower surface of the horizontal plate were “the area of the substrate /the perimeter of the substrate.” They corresponded to a characteristic length of 23 mm. The characteristic length of the vertical plate was set to 33 mm according to the height of the fin (Fig. 3a). In case of forced convection, we set a characteristic length of 80 mm for all outer surfaces of the device by assuming that air passed in the direction of the channel between the fins (Fig. 3b).

We set surface-to-surface boundary conditions for radiation on all outer surfaces of the device, and this included radiation between the outer surface of the heat sink and the environment as well as radiation

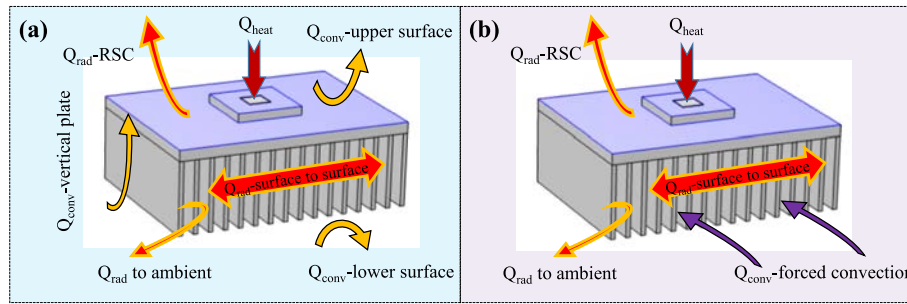


Fig. 3. Schematic diagram of boundary conditions: (a) natural convection and (b) forced convection.

within the surfaces of the device.

To ensure the accuracy of the calculations, we conducted mesh tests to arrive at appropriate mesh settings. We performed mesh tests on 3D models of different densities (from extremely coarse to ultra-fine meshes) at a concentration ratio of 100 and an ambient temperature of 25 °C in the case of natural convection. To show the results clearly, Fig. 4 depicts the relationship between the number of elements of the domain and the highest temperature of the model $T_{\text{model,max}}$ (on the surface of the solar cell) as well as its lowest temperature $T_{\text{model,min}}$ (on the surface of the heat sink). When the number of mesh elements exceeded 40,000, the maximum and minimum temperatures of the model tended to stagnate. Under the premise of affordable computational cost, we chose an ultra-fine grid for calculation containing 148,029 domain elements, 55,396 boundary elements, and 3,722 edge elements.

A steady-state solver was used to calculate the temperature and heat flux after the device had reached equilibrium, and “surface-to-surface radiation heat transfer” was used in the multi-physical field. The Generalized Minimum Residual (GMRES) iterative method was used to make the calculations more accurate.

3. Analysis of results

3.1. Contribution of RSC to heat dissipation in extremely harsh environments

Heat exchange between the device and the environment took the form of convection and radiation. Convective heat dissipation is mainly affected by wind speed and ambient temperature while radiative heat dissipation is affected by the ambient temperature only. From the perspective of heat dissipation, the worst natural environment in which solar cells operate involves an ambient temperature of 50 °C (Turpan) and a natural wind speed of 0 m/s [40]. RSC is not affected by wind speed, and the corresponding cold source is outer space with a

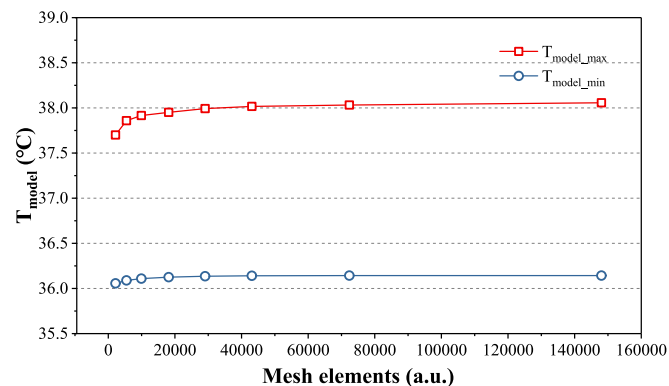


Fig. 4. Relationship between the number of mesh elements and the maximum/minimum temperature of the model.

temperature of 2.7 K, which is not affected by environmental factors. A major purpose of introducing the RCL to the design of the cooling device is to cope with the worst natural environment described above. The aim is to control the rise in the temperature of the solar cell and ensure its normal operation. Therefore, we now examine the contribution of the RSC in terms of heat dissipation when the wind speed was 0 m/s (natural convection) and the ambient temperature was 50 °C.

What we call “radiative cooling” (RC) here refers to the total radiant energy from the RCL, which in this case includes sky radiation (RSC) and conventional thermal radiation. Moreover, the “heat dissipation of the RCL” here refers to the radiant heat dissipation of the RCL unless otherwise stated.

Fig. 5(a) shows rises in the temperature of the solar cell (the highest temperature) relative to the environment, and the maximum internal difference between the temperature of the device, with and without the RCL. When the concentration ratio was 200, the cloud map device’s temperature shows that after the RCL had been laid, the surface temperatures of the solar cell, VC, and heat sink were significantly lower than those without the RCL. The RCL thus enhanced heat dissipation. The red and yellow data lines show that applying the RCL reduced the solar cell temperature by 1.76 °C compared with the case without it, and the magnitude of the reduction increased slightly with the concentration ratio. This value is relatively lower than 14 °C and 36 °C, where the radiative cooler layers were added on one and two faces of a flat heat sink, respectively [34,35]. Moreover, when the concentration ratio was lower than 8.5, the temperature of the solar cell was even lower than the ambient temperature, which is consistent with the results in the literature, but the cooling effect was not as good as that reported in the past work [27–29]. This is because in the cooling device here, the area of the RCL (part A in the figure) accounted for only 7.9 % of the total surface area of the radiator, which is much smaller than the convective and the radiative areas of heat dissipation (part A + B in the device diagram). The effect of heat dissipation of RSC was thus greatly diluted [28].

In Fig. 5(a), the difference in the internal temperature of the device $\Delta T_{\text{internal}}$ refers to the difference between the highest (on the solar cell) and the lowest temperatures (on the aluminum fin) in the heat sink. The cloud map shows that when the concentration ratio was 200 and the device did not have an RCL, the drop in temperature from the solar cell to the heat sink was only about 1 °C. This was due to the application of the TIM and VC. Their excellent thermal conductivity and uniformity of temperature caused heat to dissipate from the solar cell to the heat sink. The drop in temperature from the center to the corners of the heat sink was about 2 °C, indicating that the capacity of the heat sink for heat conduction and heat dissipation met the given requirements when the concentration ratio was 200. The effect of laying the RCL on values of $\Delta T_{\text{internal}}$ of the device was not prominent, and $\Delta T_{\text{internal}}$ was only slightly lower than that without the RCL because the overall temperature reduction due to RSC was limited (about 2 °C). The value of $\Delta T_{\text{internal}}$ of the device was approximately proportional to the concentration ratio; at a concentration ratio of 200, the value of $\Delta T_{\text{internal}}$ of the device was only 3.8 °C.

Fig. 5(b) shows the percentage of the radiation and convective heat

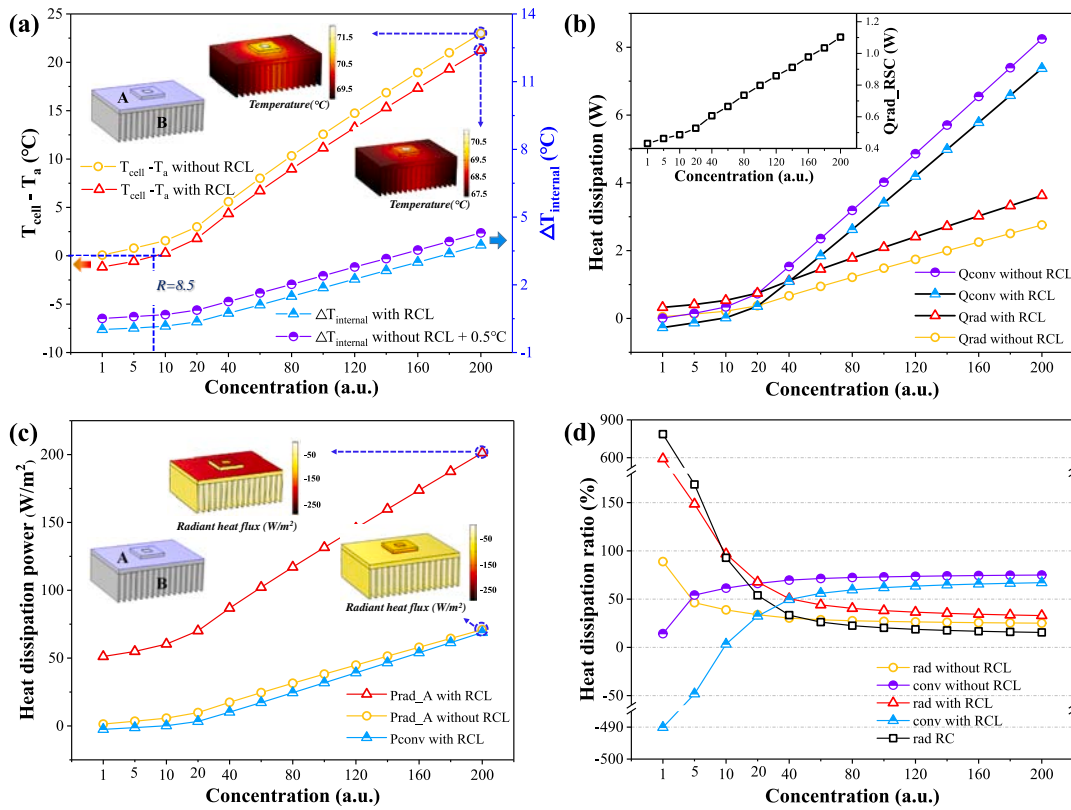


Fig. 5. Under different concentration ratios, (a) the temperature rise of the solar cell, and the maximum internal temperature difference of the device. For clear, 0.5 °C is added to the internal temperature difference of the device without RCL. The insets map the device temperature at a concentration ratio of 200. (b) The percentage of convective and radiative heat dissipation, as well as that of RSC. (c) The power of radiant and convective heat dissipation per unit area. The ambient temperature is 50 °C and the wind speed is 0 m/s.

dissipation, as well as the contribution comes from RSC, under different concentration ratio. Of them, the heat dissipation due to RSC was evaluated by the difference between the radiative heat dissipation with and without the RCL. At first, it can be observed that the heat dissipation of RSC accounts for a considerable ratio of the total radiative heat dissipation (as the concentration ratio increases, it changes from over 100 % to 15 %). Fig. 5(b) also shows that regardless of whether the RCL was added, convective heat dissipation occurred more rapidly than radiative heat dissipation with increasing rates of the concentration ratio. Therefore, the percentage of RSC-induced heat dissipation to the overall heat dissipation became small (15 %) as the concentration ratio increased to 200. However, the average power of convective heat dissipation per unit area was only 68.9 W/m² even when the concentration ratio was 200, as shown in Fig. 5(c). This value was even lower than the heat dissipation power per unit area of the surface without the RCL: 71 W/m². Fig. 5(c) also compares the radiant power of surface A when the RCL was and was not laid when the concentration ratio was 200. The radiant power per unit area of surface A with the RCL was 201 W/m², much higher than that without the RCL, 71 W/m². Therefore, the low ratio of RCL-induced heat dissipation to the total heat dissipation can be explained by the area of the RCL being much smaller than that of the other parts of the device (only 7.9 %), which diluted its heat dissipation effect. Therefore, the area/thickness ratio of the heat sink should be optimized and the ratio of the area of the front surface should be increased in the design of concentrated silicon solar cells to make better use of the cooling effect of the RSC.

3.2. Diluting effect of wind speed on the contribution of RCL

Natural wind commonly blows in the working environment of the CPV system in most cases. It significantly enhances the intensity of

convective heat dissipation and further dilutes the heat dissipation effect of the RCL while cooling the solar cell.

The typical ambient temperature is 25 °C and the ambient wind speed is in the range of 0–3 m/s. This corresponds to the vast majority of working environments of concentrated photovoltaic devices. We set the concentration ratio to 100, the ambient temperature to 25 °C, and wind speed to 0–3 m/s to investigate the effect of a dilution in convective heat dissipation on the heat dissipation-related performance of the RCL as well as the performance of the device.

Fig. 6(a) shows the rise in the temperature of the device with and without the RCL relative to the environment at different wind speeds. With the increase of wind speed from 0 m/s to 3 m/s, the temperature difference between the cell and the ambient is reduced from 13 °C to 4 °C, i.e. reduced 9 °C. The same rule was also observed when a RCL was added to a flat photovoltaic module, where the module's temperature was decreased by about 15 °C with the wind speed increasing from 0 m/s to 3 m/s [36]. The contribution of the RCL to lowering the temperature of the device fell with increasing wind speed, dropping from 1.14 °C to only 0.15 °C at wind speeds of 0 m/s and 3 m/s. This shows that the laying of the RCL still helped enhance heat dissipation but that the effect was seriously diluted. It is clear that as the wind speed increased, the rise in the temperature of the solar cell relative to the environment decreased rapidly. This shows that compared with natural convection, a minor increase in the ambient wind speed greatly enhanced the overall heat dissipation capability of the device.

Fig. 6(b) shows that as the ambient wind speed increased, the contribution of convective heat dissipation gradually increased as well. For devices without the RCL, the convective heat dissipation ratio increased from 77.8 % to 95.8 % as the wind speed increased from 0 m/s to 3 m/s. Even for devices with the RCL, the proportion of convective heat dissipation risen from 68.7 % to 88.9 %, thus contributing the most

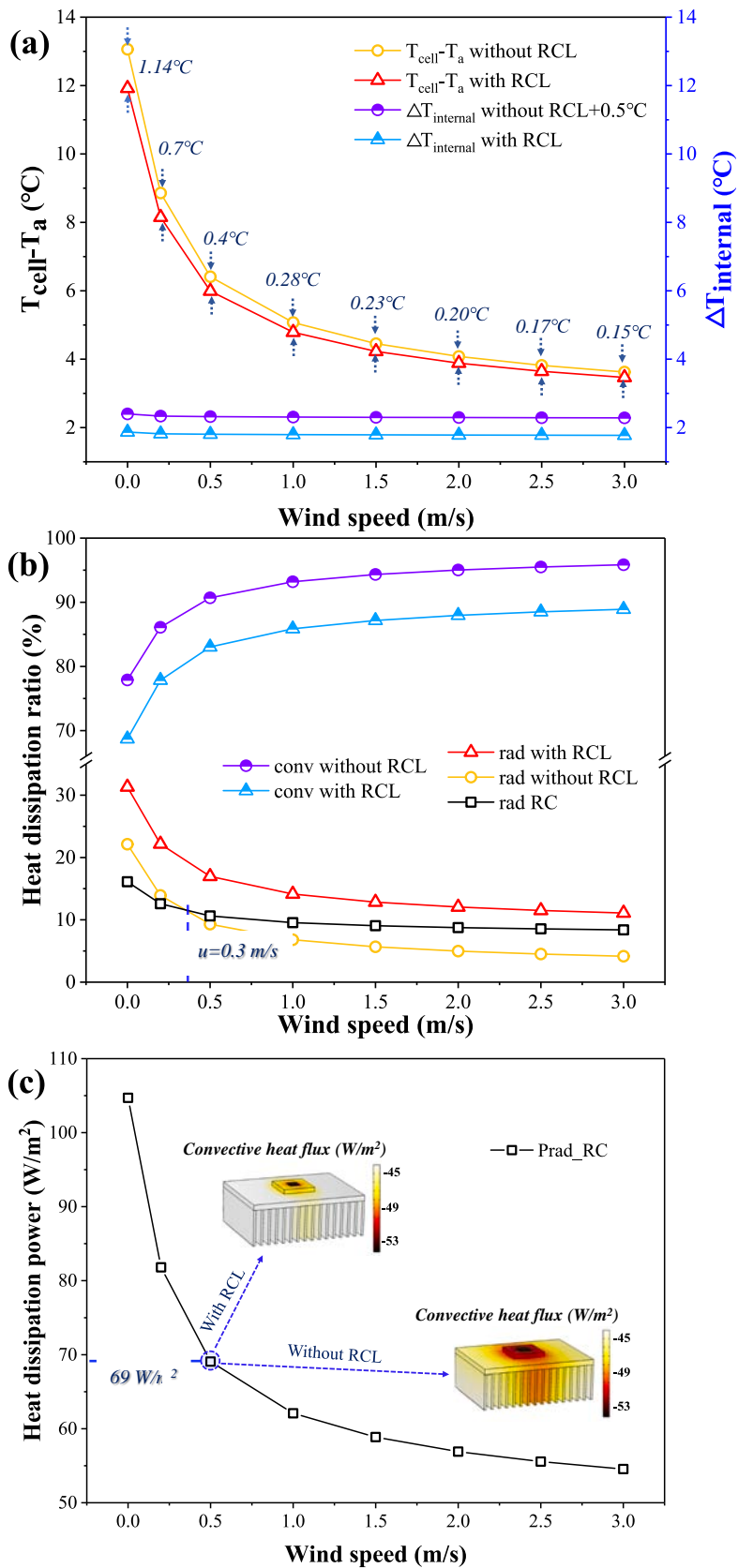


Fig. 6. With wind speed ranges from 0 to 3 m/s, (a) the temperature rise of the solar cell, and the internal temperature difference of the device; (b) the ratios of the convective and radiative heat dissipation, as well as that of RSC; (c) the RSC power per unit area of the RCL, and cloud maps of the convection power per unit area with and without RCL. The ambient temperature is 25 °C and the concentration ratio is 100.

to heat dissipation. The condition of ambient wind speed of 1 m/s can be satisfied in most weather conditions. Convection can contribute over 85 % of the heat dissipation, which confirms that our design is more valuable for CPV systems under most conditions. As shown in Fig. 6(a), the device could control a rise in the temperature of the solar cell relative to the environment of up to about 5 °C, which helped ensure that the solar cell had a suitable temperature for operation (the actual temperature was about 30 °C).

The heat dissipation effect of the RCL was diluted. On the one hand, this was owing to the rapid increase in convective heat dissipation with the increase in wind speed. On the other hand, the power of heat dissipation of the RCL decreased due to the reduction in the temperature of the device. Fig. 6(c) shows the relationship between the power radiated from per unit area of the surface of the RCL and wind speed. As the wind speed increased, the power radiated by per unit area RCL decreased rapidly: When the wind speed was 0.5 m/s, it dropped to 69 W/m², and was only 55 W/m² when the wind speed was 3 m/s. However, the RSC still played an important role in heat dissipation compared with radiation.

Fig. 6(b) shows that when the wind speed was higher than 0.3 m/s, the heat dissipation due to the RSC exceeded that owing to the thermal radiation of the device, and occupied an increasing ratio of the overall radiative heat dissipation with further increases in wind speed (when the wind speed was higher than 1.5 m/s, this ratio exceeded 70 %). Fig. 6(c) also shows that although the contribution of RSC to heat dissipation was diluted by convection, its heat dissipation power per unit area was 69 W/m² when the wind speed was 0.5 m/s, still larger than that due to convective heat dissipation (see the cloud map in Fig. 6 (c); most areas depict power per unit area under 44 W/m²). Considering the high ratio of RSC-induced heat dissipation in the case of radiative dissipation and given that its power is greater than that of convective heat dissipation, it appears that the heat dissipation capability of the CPV cooling device can be enhanced further by increasing the ratio of the area of the front surface of the heat sink. This conclusion is consistent with the previous conclusion in this study.

Fig. 6(a) also shows the values of $\Delta T_{internal}$ of the device with and without the RCL under different wind speeds. Changes in the wind speed nearly did not affect $\Delta T_{internal}$, which was stable at about 2 °C, and the effect of RCL on it was minor as well. This is because $\Delta T_{internal}$ was mainly determined by heat conduction in the solar cell-VC-heat sink channel. Such a stable $\Delta T_{internal}$ further justifies the reasonableness of the overall design of the device.

3.3. Enhancing effect of ambient temperature on the contribution of RCL

The operating temperature of the CPV system varies with seasons and the time of year. According to the expressions for convective heat transfer (Eq. (3)) and thermal radiation (Eq. (11)), the ambient temperature had a significant impact on the heat dissipation of the device. We set the concentration ratio to 100 and the wind speed to 0 m/s to investigate the influence of changes in the ambient temperature from -10 °C to 50 °C on the heat dissipation of the RSC as well as the overall heat dissipation of the device.

Fig. 7(a) shows the rise in the temperature of the device relative to the ambient temperature with and without the RCL as the ambient temperature was increased. The contribution of the RCL to reducing the temperature of the device increased from 0.79 °C to 1.42 °C with increasing ambient temperature. The higher the ambient temperature was, the more effective RCL-induced heat dissipation was because the temperature of the device increased with the ambient temperature, as shown in Fig. 7(b), which resulted in increased radiative and convective heat dissipation from the device to the environment. RSC represented radiative heat dissipation for outer space with a fixed temperature (2.7 K) and was independent of the ambient temperature. The power per unit area of RSC-induced heat dissipation increased from 72.8 W/m² to 131.5 W/m² as the device's temperature increased (Fig. 7(b)).

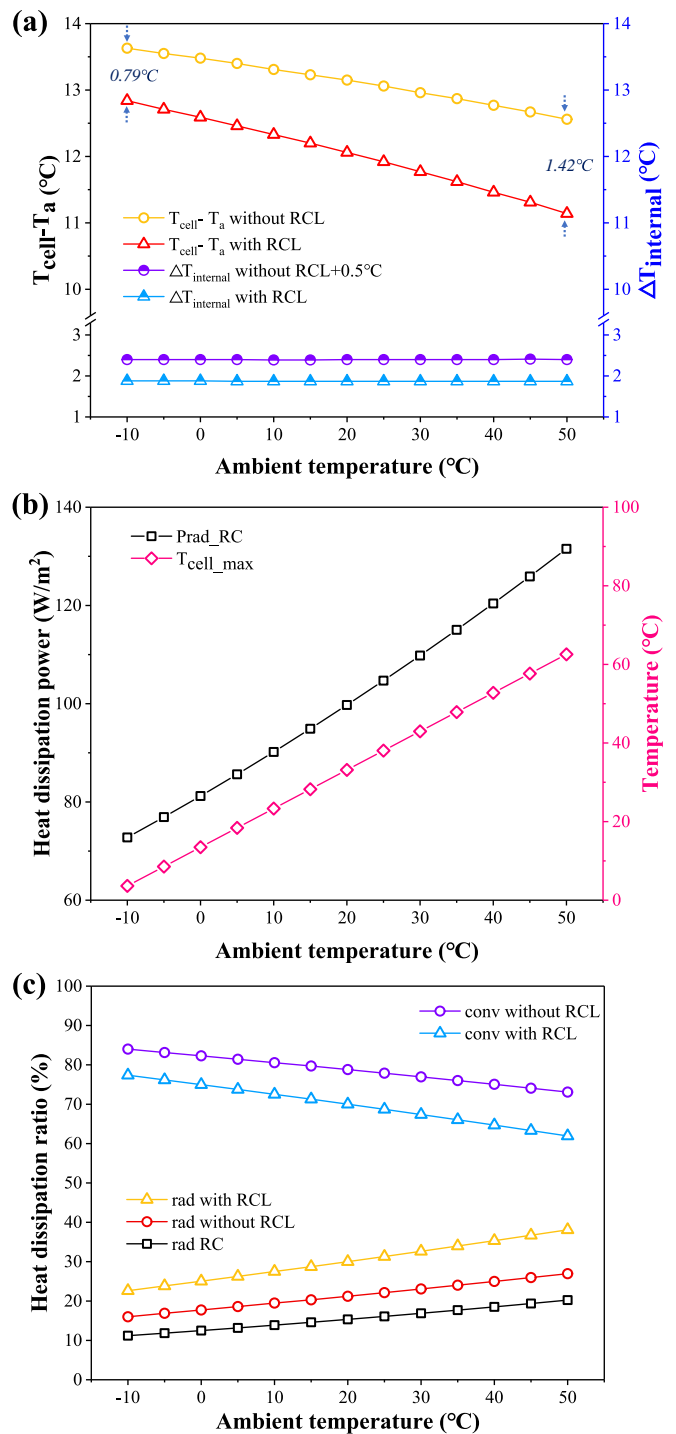


Fig. 7. With ambient temperature ranges from -10 to 50 °C, (a) the temperature rise of the solar cell, and the internal temperature difference of the device; (b) the RSC power per unit area of the RCL and the maximum temperature of the solar cell; and (c) ratios of the convective and radiative heat dissipation, as well as that of RSC. The concentration ratio was 100 and wind speed was 0 m/s.

According to Eqs. (3) and (11), the powers of heat dissipation due to thermal radiation and convection were affected by the ambient temperature. Therefore, the ratio of RSC-induced heat dissipation gradually increased with the ambient temperature, as shown in Fig. 7(c). When the ambient temperature reached 50 °C, the ratio of RSC-induced heat dissipation was 20.2 %, and it played an important role in heat dissipation in the solar cell. Considering that RCL accounted for only 7.9 % of the overall surface area of the device, increasing its area ratio could

enhance its effect in terms of heat dissipation.

Although the temperature of the device increased with the ambient temperature, as shown in Fig. 7(b), the calculations showed that this relative rise in temperature gradually decreased (Fig. 7(a)): When the device had an RCL, the temperature of the solar cell was 61.2 °C when the ambient temperature was 50 °C, only 11.2 °C higher than environmental temperature. This rule meets the requirements of the operating temperature of silicon solar cells because as the ambient temperature increased, heat flux from the device to the environment increased more quickly than from the environment to the device.

Fig. 7(c) compares the ratio of radiative and convective heat dissipation to the overall heat dissipation of the device with and without the RCL as a function of ambient temperature. It is clear that the ratio of radiative heat dissipation gradually increased with the ambient temperature, and the rate of increase for the device with the RCL was faster than that without the RCL. At the same time, the ratio of convective heat dissipation gradually decreased with the ambient temperature because radiative heat dissipation was proportional to the fourth power of the temperature (Eq. (13)). However, convection was proportional to temperature (Eq. (3)). When the device had the RCL, the radiation ratio increased more quickly for the same reason, and RSC radiated heat to a cold source at a fixed temperature, 2.7 °C.

Fig. 7(a) also presents the effect of the ambient temperature on $\Delta T_{internal}$, which remained stable at 2 °C with and without the RCL.

3.4. Maximum acceptable concentration ratio and the size of heat sink

The maximum acceptable concentration ratio is defined here as the maximum concentration multiple when the ambient wind speed is 0 m/s, and the ambient temperature is 25 °C, ensuring that the solar cell temperature does not exceed 50 °C. We examined the relationship between the size of the heat sink and the maximum acceptable concentration ratio.

The height and thickness of the heat sink were unchanged from before, and only the dimension perpendicular to the fins was allowed to be adjusted. It varied from 50 mm to 80 mm. The results are given in

Fig. 8. With and without the RCL, the relationship between the acceptable maximum concentration ratio and the heat sink size was approximately linear.

By linear fitting, the acceptable concentration ratio for devices with the RCL can be given as follows:

$$CR_{with\ RCL} = 41.607 + 2.336 \cdot L_{heat-sink} \quad (14)$$

By linear fitting, the acceptable concentration ratio for devices without the RCL is as follows:

$$CR_{without\ RCL} = 40.036 + 2.164 \cdot L_{heat-sink} \quad (15)$$

When the RCL was added, the device could withstand a concentration ratio higher by at least 10 than without the RCL. This gap increased with the size of the heat sink.

Thus, the RCL can significantly enhance heat dissipation in LM-CPV systems. Under the worst conditions (wind speed of 0 m/s and ambient temperature of 50 °C), the ratio of RSC-induced heat dissipation (Fig. 5 (b)) exceeded 15 % when the concentration ratio was 200. This ratio could guarantee that solar cell did not exceed 71.5 °C (Fig. 5(a)) and could operate normally. When the concentration ratio was 100, the percentage of RSC-induced heat dissipation was 20.2 %, the solar cell could be maintained at 61.2 °C. In most weather conditions (wind speed of 1 m/s and ambient temperature of 25 °C), thermal convection significantly dilutes the effect of RSC, but the overall heat dissipation effect substantially improves. When the concentration ratio was 100, the proposed cooling device could guarantee that the solar cells could operate at a temperature of around 30 °C. The relation between the maximum concentration ratio acceptable for the normal operation of the device and the heat sink's size was approximately linear. Moreover, the difference in temperature within the device could be controlled within 3.8 °C.

4. Conclusions

In this paper, we proposed a passive cooling device for LM-CPV systems combining a RCL and a finned heat sink, which can not only

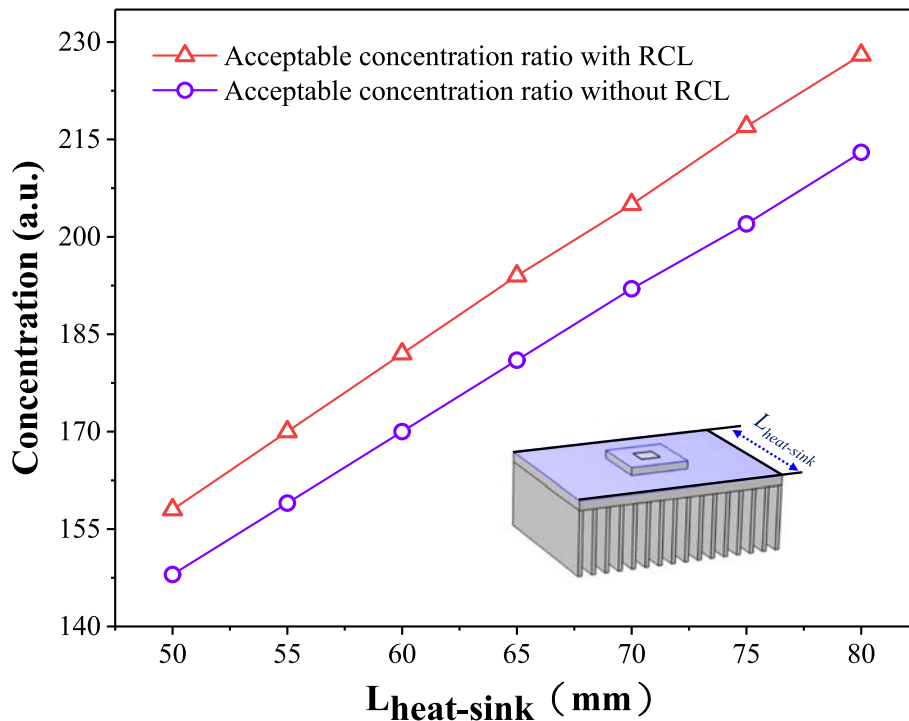


Fig. 8. Relationship between the acceptable concentration ratio and the heat sink size when the ambient temperature is 25 °C, the wind speed is 0 m/s, and the cell temperature is 50 °C.

give play to the heat dissipation effect of the RSC but also give full play to the role of convection heat dissipation. Based on numerical simulations, we examined the contribution of RSC to the drop in temperature and heat dissipation of the device while considering the effects of the wind speed, ambient temperature, and concentration ratio. The results showed that RSC could play an important role in enhancing heat dissipation in LM-CPV systems. When the concentration ratio was 100, under the worst conditions for heat dissipation (wind speed of 0 m/s and ambient temperature of 50 °C), the ratio of RSC-induced heat dissipation to total heat dissipation exceeded 20.2 %, which guaranteed that the temperature of the solar cells did not exceed 61.2 °C. While in most conditions (wind speed of 1 m/s and ambient temperature of 25 °C), RSC can still significantly improve the heat dissipation of the device (contribute 9.55 %), which could guarantee the solar cells worked at temperatures around 30 °C.

The increase in wind speed significantly diluted the heat dissipation of RSC. When the concentration ratio was 100 and the ambient temperature was 25 °C, the percentage of RSC to overall heat dissipation decreased from 16.1 % to 8.4 % as the wind speed increased from 0 m/s to 3 m/s. The ambient temperature increases significantly increased the ratio of RSC to the overall heat dissipation. When the concentration ratio was 100 and wind speed was 0 m/s, the ambient temperature increased from −10 °C to 50 °C, and the contribution of the RCL to the drop in the temperature of the device increased from 0.79 °C to 1.42 °C. The maximum concentration ratio acceptable for the device was approximately linear with respect to the size of the heat sink, and the LM-CPV system with RCL could withstand a concentration ratio of 10 to 15 higher than that without the RCL.

The low ratio of RSC to the total heat dissipation mainly attributes to the area of RCL being much smaller than that of other parts. However, the heat dissipation power per unit area of the RCL far exceeded that of thermal convection and radiation. An optimized LM-CPV system can be obtained by increasing the area ratio of the RCL. This work provides a stable and reliable technical choice for reducing the cost and increasing the efficiency of photovoltaic power generation.

Declaration of Competing Interest

The authors declare that they have no known competing financial interests or personal relationships that could have appeared to influence the work reported in this paper.

Data availability

No data was used for the research described in the article.

Acknowledgements

This work is supported partially by National Natural Science Foundation of China (Grant nos. 52072121, 52232008, 51972110, and 52102245), Beijing Natural Science Foundation (2222076, 2222077), Beijing Science and Technology Project (Z211100004621010), project of State Key Laboratory of Alternate Electrical Power System with Renewable Energy Sources (LAPS202114), the project named key technologies of intelligent joint regulation and operation with grid connected friendly in power station group of wind, solar photovoltaic and energy storage, sponsored by China Three Gorges Corporation (WWKY-2021-0173), 2022 Strategic Research Key Project of Science and Technology Commission of the Ministry of Education, Huaneng Group Headquarters Science and Technology Project (HNKJ20-H88), the Fundamental Research Funds for the Central Universities (2020MS023, 2022MS029, 2022MS02, 2022MS031) and the NCEPU "Double First-Class" Program.

References

- [1] IMS Research, Available at: <https://www.researchandmarkets.com/research/hsnh/b6/concentrated>, 2012.
- [2] M.A. Green, et al., Solar cell efficiency tables (version 54), *Prog. Photovoltaics Res. Appl.* 27 (7) (2019) 565.
- [3] P. Campbell, et al., The limiting efficiency of silicon solar cells under concentrated sunlight, *IEEE Trans. Electron. Devices* 33 (2) (1986) 234.
- [4] F. Mavromatakis, et al., Low irradiance losses of photovoltaic modules, *Sol. Energy* 157 (2017) 496.
- [5] M. Ahmed, et al., Performance evaluation of new modified low-concentrator polycrystalline silicon photovoltaic/thermal systems, *Energy Convers. Manage.* 149 (2017) 593.
- [6] S. Yoon et al., Reduced temperature dependence of high-concentration photovoltaic solar cell open-circuit voltage (Voc) at high concentration levels, in: *IEEE First World Conference on Photovoltaic Energy Conversion, Conference Record of the Twenty Fourth IEEE Photovoltaic Specialists Conference IEEE*, 1994.
- [7] F. Bayrak, et al., Effects of different fin parameters on temperature and efficiency for cooling of photovoltaic panels under natural convection, *Sol. Energy* 188 (2019) 484.
- [8] A.P. Raman, et al., Passive radiative cooling below ambient air temperature under direct sunlight, *Nature* 515 (7528) (2014) 540.
- [9] X. Wang, et al., Scalable flexible hybrid membranes with photonic structures for daytime radiative cooling, *Adv. Funct. Mater.* 30 (5) (2020) 1907562.
- [10] Y. Fu, et al., Daytime passive radiative cooler using porous alumina, *Sol. Energy Mater. Sol. Cells* 191 (2019) 50–54.
- [11] S.Y. Jeong, et al., Daytime passive radiative cooling by ultra emissive bio-inspired polymeric surface, *Sol. Energy Mater. Sol. Cells* 206 (2020), 110296.
- [12] B. Zhao, et al., Radiative cooling: A review of fundamentals, materials, applications, and prospects, *Appl. Energy* 236 (2019) 489–513.
- [13] C. Sheng, et al., Colored radiative cooler under optical Tamm resonance, *ACS Photonics* 6 (10) (2019) 2545–2552.
- [14] J. Mandal, et al., Hierarchically porous polymer coatings for highly efficient passive daytime radiative cooling, *Science* 362 (6412) (2018) 315–319.
- [15] N.N. Shi, et al., Keeping cool: Enhanced optical reflection and radiative heat dissipation in Saharan silver ants, *Science* 349 (6245) (2015) 298–301.
- [16] G. Silva-Oelker, et al., Numerical study of sodalime and PDMS hemisphere photonic structures for radiative cooling of silicon solar cells, *Opt. Express* 30 (18) (2022) 32965–32977.
- [17] Y. Zhai, et al., Scalable-manufactured randomized glass-polymer hybrid metamaterial for daytime radiative cooling, *Science* 355 (6329) (2017) 1062–1066.
- [18] M.A. Kecebas, et al., Passive radiative cooling design with broadband optical thin-film filters, *J. Quant. Spectrosc. Radiat. Transf.* 198 (2017) 179–186.
- [19] Y. Huang, et al., Broadband metamaterial as an “invisible” radiative cooling coat, *Opt. Commun.* 407 (2018) 204–207.
- [20] X. Yu, et al., A simulation study for comparing the cooling performance of different daytime radiative cooling materials, *Sol. Energy Mater. Sol. Cells* 209 (2020), 110459.
- [21] S. Meng, et al., Scalable dual-layer film with broadband infrared emission for sub-ambient daytime radiative cooling, *Sol. Energy Mater. Sol. Cells* 208 (2020), 110393.
- [22] M. Chen, et al., Passive daytime radiative cooling: Fundamentals, material designs, and applications, *EcoMat* 4 (1) (2022) e12153.
- [23] B. Zhao, et al., Sub-ambient daytime radiative cooling based on continuous sunlight blocking, *Sol. Energy Mater. Sol. Cells* 245 (2022), 111854.
- [24] J. Dumoulin, et al., Radiative sky cooling of solar cells: fundamental modelling and cooling potential of single-junction devices, *Sustain. Energy & Fuels* 5 (7) (2021) 2085–2096.
- [25] G. Perrakis, et al., Combined nano and micro structuring for enhanced radiative cooling and efficiency of photovoltaic cells, *Sci. Reports* 11 (1) (2021) 1–10.
- [26] G. Chen, et al., A visibly transparent radiative cooling film with self-cleaning function produced by solution processing, *J. Mater. Sci. Technol.* 90 (2021) 76–84.
- [27] L. Zhu, et al., Radiative cooling of solar cells, *Optica* 1 (1) (2014) 32–38.
- [28] L. Zhu, et al., Radiative cooling of solar absorbers using a visibly transparent photonic crystal thermal blackbody, *Proc. Natl. Acad. Sci.* 112 (40) (2015) 12282.
- [29] W. Li, et al., A comprehensive photonic approach for solar cell cooling, *ACS Photonics* 4 (4) (2017) 774–782.
- [30] K. Wang, et al., Radiative cooling of commercial silicon solar cells using a pyramid-textured PDMS film, *Sol. Energy* 225 (2021) 245–251.
- [31] B. Zhao, et al., Radiative cooling of solar cells with micro-grating photonic cooler, *Renew. Energy* 191 (2022) 662–668.
- [32] X. Sun, et al., Optics-based approach to thermal management of photovoltaics: Selective-spectral and radiative cooling, *IEEE J. Photovoltaics* 7 (2) (2017) 566.
- [33] K.W. Lee, et al., Visibly Clear Radiative Cooling Metamaterials for Enhanced Thermal Management in Solar Cells and Windows, *Adv. Funct. Mater.* 32 (1) (2022) 2105882.
- [34] Y. Sun, et al., Radiative cooling for concentrating photovoltaic systems, *In Therm. Radiat. Manag. Energy Appl.* 10369 (2017) 25–34.
- [35] Z. Wang, et al., Lightweight, passive radiative cooling to enhance concentrating photovoltaics, *Joule* 4 (12) (2020) 2702–2717.
- [36] Z. Li, et al., Investigating the effect of radiative cooling on the operating temperature of photovoltaic modules, *Sol. RRL* 5 (4) (2021) 2000735.
- [37] J. Liu, et al., Recent advances in the development of radiative sky cooling inspired from solar thermal harvesting, *Nano Energy* 81 (2021), 105611.

- [38] S. Ahmed, et al., Enhanced radiative cooling of solar cells by integration with heat pipe, *Appl. Energy* 308 (2022), 118363.
- [39] G.J. Huang, et al., Dynamic characteristics of natural convection from horizontal rectangular fin arrays, *Appl. Therm. Eng.* 42 (2012) 81–89.
- [40] K. Xiao, et al., Atmospheric corrosion factors of printed circuit boards in a dry-heat desert environment: Salty dust and diurnal temperature difference, *Chem. Eng. J.* 336 (2018) 92–101.
- [41] A. Aldossary, et al., Technical feasibility study of passive and active cooling for concentrator PV in harsh environment, *Appl. Therm. Eng.* 490–500 (2016).
- [42] M.J. Rightley, et al., Innovative wick design for multi-source, flat plate heat pipes, *Microelectron. J.* 34 (3) (2003) 187–194.
- [43] M.A. Bramson, *Infrared radiation. A handbook for applications*, Opt. Phys. Eng., (1968).
- [44] C. Oahman, *Emittance measurements using AGEMA E-Box*, Tech. Rep., AGEMA (1999).
- [45] T. Kerzmann, et al., System simulation of a linear concentrating photovoltaic system with an active cooling system, *Renew. Energy* 41 (2012) 254–261.
- [46] Z. Huang, et al., Nanoparticle embedded double-layer coating for daytime radiative cooling, *Int. J. Heat Mass Transf.* 104 (2017) 890–896.
- [47] H. Bao, et al., Double-layer nanoparticle-based coatings for efficient terrestrial radiative cooling, *Sol. Energy Mater. Sol. Cells* 168 (2017) 78–84.
- [48] B. Zhao, et al., Comprehensive photonic approach for diurnal photovoltaic and nocturnal radiative cooling, *Sol. Energy Mater. Sol. Cells* 178 (2018) 266–272.
- [49] P. Berdahl, et al., The thermal radiance of clear skies, *Sol. Energy* 29 (1982) 299–314.
- [50] D.L. Zhao, et al., Radiative sky cooling: fundamental principles, materials, and applications, *Appl. Phys. Rev.* 6 (2) (2019), 021306.
- [51] B. Zhao, *Study on radiative sky cooling and its coupling utilization with solar photovoltaic conversion*. Diss. University of Science and Technology of China, 2020.
- [52] S.-H. Yu, et al., Natural convection around a radial heat sink, *Int. J. Heat Mass Transf.* 53 (13–14) (2010) 2935–2938.
- [53] M. Theristis, et al., Design and numerical analysis of enhanced cooling techniques for a high concentration photovoltaic (HCPV) system, *27th European Photovolt. Sol. Energy Conf. and Exhib.* (2012).
- [54] F.P. Incropera et al., *Fundam. Heat Mass Transf.*, 6th ed., John Wiley & Sons, 2006.
- [55] Z. Min, et al., Investigation of thermal radiation effects on solid oxide fuel cell performance by a comprehensive model, *J. Power Sources* 206 (2012) 185–196.